Journal of Sound and Vibration (1998) **210**(4), 415–429

FREQUENCY ANALYSIS OF A ROTATING PLATE WITH EXTERNAL BEAM-SUPPORTS

S.-C. HUANG AND C.-H. WU

Department of Mechanical Engineering, National Taiwan University of Science and Technology 43 *Keelung Road, Sec.* 4, *Taipei, Taiwan* 106, *Republic of China*

(*Received* 26 *February* 1995, *and in final form* 19 *October* 1995)

The vibration characteristics of a rotating plate with external, radial beam-supports is studied. A new approach that employs a mixed weighted residual method and the receptance method is introduced. Numerical examples follow to demonstrate the approach and to show the variations of natural frequencies and critical speeds with rotation speed. The results show that the beam-supports can raise some of plate's natural frequencies. The improvement of the first critical speed, however, relies on the number and placement of supports. The beam-supports are further found to introduce additional critical speeds after the first critical speed. Effects on the natural frequencies and critical speeds, due to support stiffness and inertia ratios to the plate, are also discussed. It is shown that higher modes are more sensitive to the supports' properties.

1. INTRODUCTION

Rotating plates are of widespread occurrence in engineering applications: as, e.g., saw blades, turbines, flywheels and computer disks. Hence, the vibration characteristics of rotating plates have been investigated for years. Lamb and Southwell [1] derived the equations for a rotating plate and solved for the natural frequencies and mode shapes. Mote [2] employed the Rayleigh–Ritz method for the vibrations of disks with initial stresses. Ramaiah [3] used the same method and analyzed rotating plates of eight different combinations of boundary conditions. Adams [4] looked into the critical speeds of spinning disks.

Lately, more researchers have focused on the dynamic behaviour of plates and their connected structures. For instance, Shen and Mote [5] and Chen and Bogy [6, 7] discussed the rotating plate with a stationary spring–mass–dashpot load to simulate a rotating disk-head assembly. Leissa and Kirk [8] and Sinha [9] investigated the vibrations of a plate with an outer ring reinforcement. Loh and Carney [10] discussed a plate with edge beams reinforcement. Some research contributed to the vibration of plate with external supports. Azimi extensively analyzed the vibration of a non-rotating plate with elastic edge supports [11], with interior supports [12], and with point supports [13]. Huang and Hsu further discussed the rotating plate with interior point supports [14] and with interior circular line supports [15]. In references [11–15] the receptance method was utilized.

In Figure 1 is shown a rotating plate with external, radial beam-supports. To the authors' knowledge, there have been no studies concerning this system. The present research is hence to develop an approach for the natural frequency analysis. The plate is assumed to have a fixed-free boundary and to rotate at a constant speed Ω. The external

0022–460X/98/090415 + 15 $25.00/0/sv951337

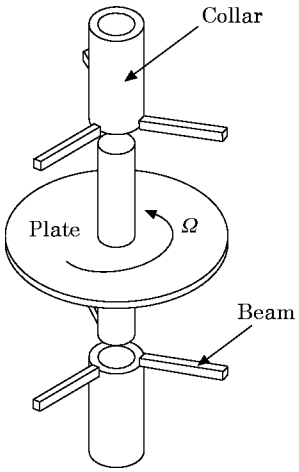

Figure 1. A rotating plate with beam-supports on both sides.

beam-supports, connected to collars, are assumed to have the same boundary as the plate. Moreover, the supports are assumed to provide a radial line restraint to the plate's transverse vibration: i.e., the contact friction is neglected.

The approach first employs a mixed weighted residual method to discretize the equations, and then introduces the receptance method for the plate-supports connection. Numerical examples for two to four supports are illustrated. Provided that the

TABLE 1

The plate's natural frequencies ω^*, *compared with those of Vogel and Skinner* (*in square brackets*)

		Clamping ratio, b/a				
m	n	0·1	0·3	0·5	0·7	0·9
0	0	4.23 [4·24]	6·67 [6·66]	13·03 [13·03]	36·95 [36·95]	344·34 [344·40]
0	1	3·50 [3·48]	6·55 [6·55]	13·29 [13·29]	37·50 [37·50]	345·10 [345·17]
0	2	5·65 [5·62]	7·96 [7·96]	14·70 [14·71]	39·27 [39·28]	347·40 [347·47]
0	3	12·51 [12·45]	13·32 [13·28]	18·58 [18·56]	42·65 [42·66]	351·32 [351·32]
1	0	25·35 [25·26]	42·63 [42·62]	85·03 [85·03]	239·85 [239·84]	2188·83 [2188·82]
1	1	27·78 [27·67]	44·65 [44·63]	86·71 [86·71]	241·25 [241·28]	2189·69 [2190·10]
1	2	37·02 [36·94]	50·97 [50·95]	91·74 [91·74]	245·55 [245·59]	2193·50 [2193·92]
1	3	53·23 [53·20]	62·09 [62·05]	100·17 [100·17]	252·70 [252·73]	2199·86 [2200·29]

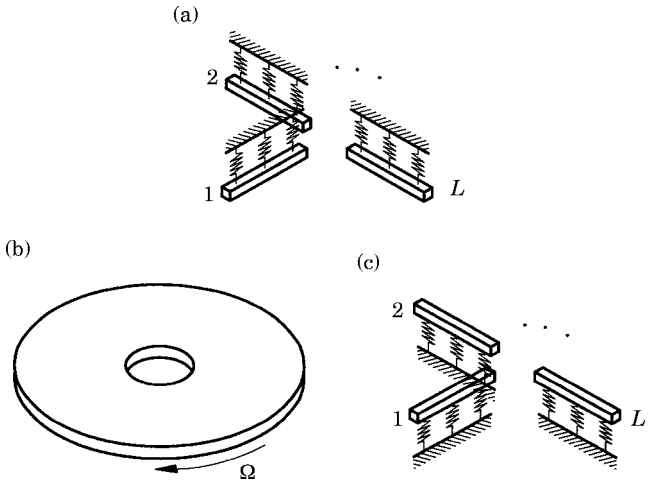

Figure 2. Decomposition of the beam-supported rotating plate.

beams and plate are of the same material and thickness, numerical results show that the plate's lowest few natural frequencies are raised by the beam-supports. The plate's first critical speed, however, is not always improved by the beam-supports. If the improvement of critical speed is the major concern, the number of supports should be carefully chosen to avoid the coincidence of supports with nodal diameters of the critical mode. Finally, the variations of natural frequencies and critical speeds due to support stiffness and inertia are discussed.

2. ROTATING PLATE EQUATIONS

A plate, of inner radius b, outer radius a, thickness h_p, density ρ_p, bending rigidity, $D = E_p h_p^3/12(1-\nu^2)$ and rotation speed Ω, has the transverse vibration equation [14–16],

$$D\nabla^4 u - \frac{h_p}{r}\left[\frac{\partial}{\partial r}\left(\sigma^r r\,\frac{\partial u}{\partial r}\right) + \frac{\partial}{\partial \phi}\left(\sigma^\phi\,\frac{\partial u}{r\,\partial \phi}\right)\right] + \rho_p h_p\left[\frac{\partial^2 u}{\partial t^2} + 2\Omega\,\frac{\partial^2 u}{\partial \phi \partial t} + \Omega^2\,\frac{\partial^2 u}{\partial \phi^2}\right] = q(r,\phi,t), \tag{1}$$

where $u(r, \phi, t)$ denotes the transverse displacement with respect to the inertia (r, ϕ) frame, and the biharmonic operator is of the form

$$\nabla^4 = \left(\frac{\partial^2}{\partial r^2} + \frac{\partial}{r\partial r} + \frac{1}{r^2}\frac{\partial^2}{\partial \phi^2}\right)^2. \tag{2}$$

The initial stresses resulting from rotation [14–16] are

$$\sigma^r(r,\Omega) = \frac{(3+\nu)}{8}\rho_p\Omega^2(a^2-r^2) + \frac{\rho_p\Omega^2 b^2(1-\nu)[a^2(3+\nu)-b^2(1+\nu)]}{8[b^2(1-\nu)+a^2(1+\nu)]}\left(\frac{a^2}{r^2}-1\right), \tag{3}$$

$$\sigma^\phi(r,\Omega) = \frac{\rho_p\Omega^2}{8}[(3+\nu)a^2-(1+3\nu)r^2]$$

$$-\frac{\rho_p\Omega^2 b^2(1-\nu)[a^2(3+\nu)-b^2(1+\nu)]}{8[b^2(1-\nu)+a^2(1+\nu)]}\left(\frac{a^2}{r^2}+1\right), \tag{4}$$

The clamped–free boundaries are

$$-D\left[\frac{\partial^2 u}{\partial r^2}+v\left(\frac{1}{r}\frac{\partial u}{\partial r}+\frac{1}{r^2}\frac{\partial^2 u}{\partial \phi^2}\right)\right]_{r=a}=0, \tag{5}$$

$$-D\left[\frac{\partial}{\partial r}(\nabla^2 u)+\frac{(1-v)}{r}\frac{\partial^2}{\partial r\,\partial \phi}\left(\frac{1}{r}\frac{\partial u}{\partial \phi}\right)\right]_{r=a}=0, \tag{6}$$

$$u(r,\phi,t)\big|_{r=b}=0, \tag{7}$$

$$\left.\frac{\partial u(r,\phi,t)}{\partial r}\right|_{r=b}=0. \tag{8}$$

First, from the modal expansion theory, the response of the spinning disk can be expressed as

$$u(r,\phi,t)=\sum_{m=0}^{M}\sum_{n=0}^{N}[q^c_{mn}(t)\cos n\phi+q^s_{mn}(t)\sin n\phi]R_{mn}(r), \tag{9}$$

where $q^c_{mn}(t)$ and $q^s_{mn}(t)$ denote two undetermined, independent generalized co-ordinates. Due to the existence of rotation, searching for exact solutions of $R_{mn}(r)$ is infeasible. Some researchers, e.g., Hutton *et al*. [14] and Huang and Hsu [12, 13] have used polynomial functions. Lately, Huang and Chiou [15] have selected modified beam functions that satisfied all the plate boundaries to solve for the plate responses due to radially travelling forces and obtained satisfactory results. The present research selects the straight beam functions for $R_{mn}(r)$; i.e.,

$$R_m(r)=[\sin\beta_m(r-b)-\sinh\beta_m(r-b)]+\alpha_m[\cos\beta_m(r-b)-\cosh\beta_m(r-b)]. \tag{10}$$

The selected functions satisfy the inner boundaries. They are functions of m (the nodal circle) and yet are independent of n (the nodal diameter). Therefore, there exist not only the interior but also the boundary residuals. A mixed weighted residual method is hence applied.

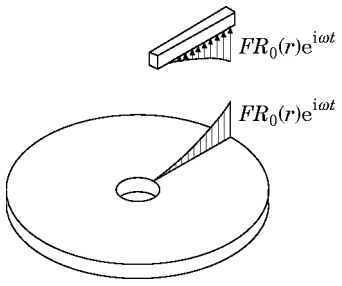

Figure 3. A line load between the beam and the plate.

TABLE 2

The geometric and material properties of the plate and the beam

Density, ρ	$7{\cdot}85 \times 10^3$ kg/m^3
Young's modulus, E	$2{\cdot}6 \times 10^9$ N/m^2
Poisson's ratio, v	0·3
Thickness, h_p, h_b	3·0 mm
Outer radius, a	100·0 mm
Inner radius, b	30·0 mm

The residuals of the plate are now defined as

$$e_I = L[u] + \rho_p h_p \left[\frac{\partial^2 u}{\partial t^2} + 2\Omega \frac{\partial^2 u}{\partial \phi \, \partial t} + \Omega^2 \frac{\partial^2 u}{\partial \phi^2} \right] - q(r, \phi, t),$$

$$e_M = B_M[u],$$

$$e_V = B_V[u], \tag{11}$$

where L and B are linear differential operators:

$$L = D\left(\frac{\mathrm{d}^2}{\mathrm{d}r^2} + \frac{\mathrm{d}}{r\,\mathrm{d}r} - \frac{n^2}{r^2} \right)^2 - \frac{h_p}{r} \left[\frac{\mathrm{d}}{\mathrm{d}r} \left(\sigma^r r \frac{\mathrm{d}}{\mathrm{d}r} \right) - \frac{n^2}{r} \sigma^\phi \right], \tag{12}$$

$$B_M = -D \left[\frac{\mathrm{d}^2}{\mathrm{d}r^2} + \frac{v}{r} \frac{\mathrm{d}}{\mathrm{d}r} - \frac{v n^2}{r^2} \right]_{r=a}, \tag{13}$$

$$B_V = -D \left[\frac{\mathrm{d}^3}{\mathrm{d}r^3} + \frac{1}{r} \frac{\mathrm{d}^2}{\mathrm{d}r^2} - \frac{1 + n^2(1-v)}{r^2} \frac{\mathrm{d}}{\mathrm{d}r} + \frac{n^2(3-v)}{r^3} \right]_{r=a}. \tag{14}$$

The sum of the weighted residuals is required to be zero: i.e.,

$$\int_b^a R_m(r) \cdot e_I \cdot r \, \mathrm{d}r + \left[r + \frac{dR_m(r)}{\mathrm{d}r} \right]_{r=a} e_M + [rR_m]_{r=a} \, e_V = 0, \qquad m = 0, 1, 2, \ldots . \tag{15}$$

TABLE 3

The beam and plate $m = 0$ natural frequencies

	Plate			
Beam	$n = 0$	$n = 1$	$n = 2$	$n = 3$
8·62	6·67	6·55	7·96	13·32

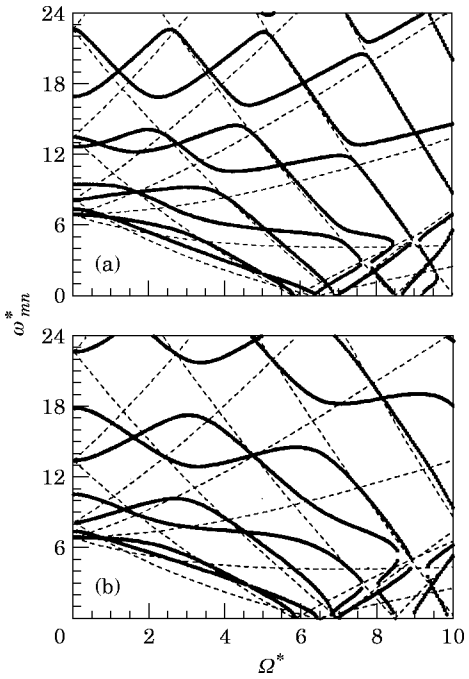

Figure 4. Variations of natural frequencies with rotation speeds for $L = 2$. (a) $k = 2000$ N/m^2; (b) $k = \infty$.

The test functions are chosen so that all the boundary residuals yield consistent units. After rearrangement, a set of differential equations for each n yields

$$\sum_{m=0}^{M} (\Gamma_{sm0}\ddot{q}^c_{m0} + \Phi_{sm0}q^c_{m0}) = Q_{s0}, \qquad n = 0, \tag{16}$$

$$\sum_{m=0}^{M} \{\Gamma_{smn}\mathbf{I}\ddot{\boldsymbol{q}}_{mn} + \Gamma_{smn}\boldsymbol{G}_n\ddot{\boldsymbol{q}}_{mn} + (\boldsymbol{\Phi}_{smn} - n^2\Omega^2\Gamma_{smn})\mathbf{I}\boldsymbol{q}_{mn}\} = \mathbf{Q}_{sn},$$

$$n > 0, \quad s = 0, 1, 2, \ldots, M, \tag{17}$$

where $\mathbf{I}$ is a 2×2 unit matrix and

$$\Gamma_{smn} = \int_b^a R_m(r)R_s(r)r \, \mathrm{d}r, \tag{18}$$

$$\Phi_{smn} = \frac{1}{\rho_p h_p}\left\{\int_b^a L[R_m]R_s r \, \mathrm{d}r + B_M[R_m]\left[r\frac{\mathrm{d}R_m(r)}{\mathrm{d}r}\right]_{r=a} + B_V[R_m][rR_m]_{r=a}\right\}, \tag{19}$$

$$\mathbf{q}_{mn} = \begin{Bmatrix} q^s_{mn} \\ q^c_{mn} \end{Bmatrix}, \qquad \mathbf{G}_n = \begin{bmatrix} 0 & -2n\Omega \\ 2n\Omega & 0 \end{bmatrix}, \tag{20}$$

$$Q_{s0} = \frac{1}{2\rho_p h_p \pi} \int_b^a \int_0^{2\pi} R_s(r) q(r, \phi, t) r \, \mathrm{d}\phi \, \mathrm{d}r, \tag{21}$$

$$\mathbf{Q}_{sn} = \frac{1}{\rho_p h_p \pi} \int_b^a \int_0^{2\pi} R_s(r) q(r, \phi, t) r \begin{Bmatrix} \sin(n\phi) \\ \cos(n\phi) \end{Bmatrix} \mathrm{d}\phi \, \mathrm{d}r. \tag{22}$$

Equation (17) yields a $2(M+1)$ order differential equations for each n. The natural frequencies of $m = 0, 1$, $n = 0, \ldots, 3$ were first solved by using a four-term ($M = 3$) approximation. The dimensionless frequencies, i.e., $\omega^* = \omega(\rho_p h_p a^4/D)^{1/2}$, are shown in Table 1 and compared to those of Vogel [18]. The comparisons show excellent accuracy of the present approach. The $m = 0$ (zero nodal circle) modes of the plate are the fundamentals and usually of primary interest. Numerical results have shown that if one merely uses a one-term $M = 0$ approximation, the errors compared to the four-term results fell below 3% for a large range of clamping ratios. Thus, only the one-term approximation need be considered when solving for the $m = 0$ modes. The equations are consequently simplified to be

$$\ddot{q}_0^c(t) + \Psi_0^2 q_0^c(t) = Q_0/\Gamma_0, \qquad n = 0, \tag{23}$$

$$\begin{Bmatrix} \ddot{q}_n^s \\ \ddot{q}_n^c \end{Bmatrix} + \begin{bmatrix} 0 & -2n\Omega \\ 2n\Omega & 0 \end{bmatrix} \begin{Bmatrix} \dot{q}_n^s \\ \dot{q}_n^c \end{Bmatrix} + \begin{bmatrix} \Psi_n^2 - n^2\Omega^2 & 0 \\ 0 & \Psi_n^2 - n^2\Omega^2 \end{bmatrix} \begin{Bmatrix} q_n^s \\ q_n^c \end{Bmatrix} = \frac{\mathbf{Q}_n}{\Gamma_n}, \qquad n \neq 0 \tag{24}$$

where $\Psi_n^2 = \Phi_n/\Gamma_n$. The subscripts s and m, both representing nodal circle number, are dropped hereafter.

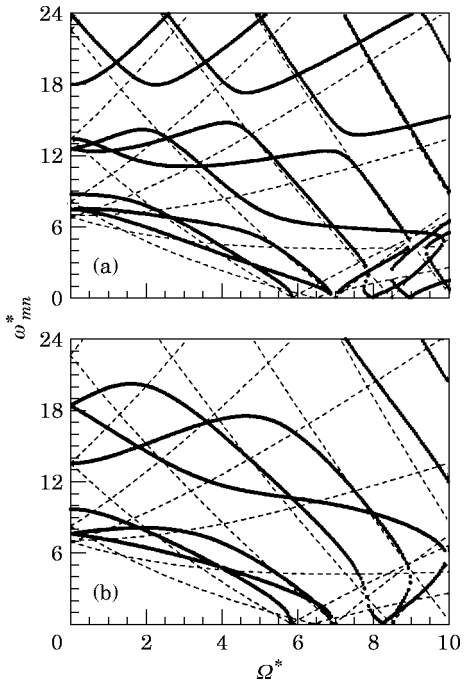

Figure 5. Variations of natural frequencies with rotation speeds for $L = 3$. (a), (b) as Figure 4.

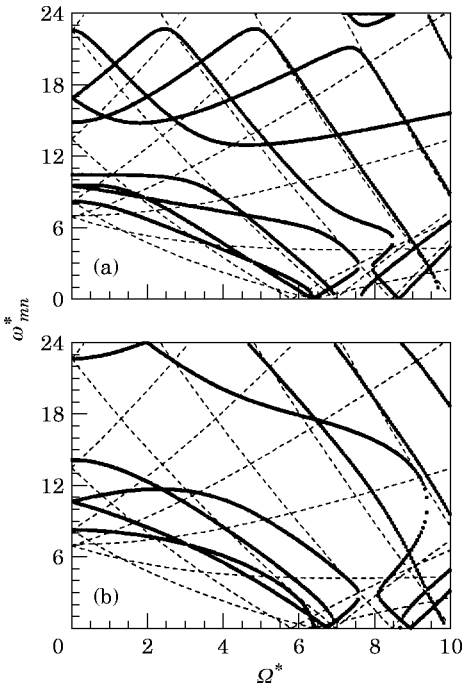

Figure 6. Variations of natural frequencies with rotation speeds for $L = 4$. (a), (b) as Figure 4.

3. BEAM EQUATIONS

Each support is treated as a clamped–free beam and it restricts the plate's transverse deflection. The distributed stiffness $k(r)$ presents an additional external stiffness. One could let k go to infinity if the supports were rigid. The equation of motion for the beam is

$$(E_b I_b\, \partial^4 u/\partial r^4) + k(r)u + \rho_b A_b\, \partial^2 u/\partial t^2 = f(r, t), \tag{25}$$

where $u(r, t)$ and $f(t)$ denote transverse displacement and the applied load. In the same manner,

$$u(r, t) = \sum_{m=0}^{M} n_m(t)\ R_m(r). \tag{26}$$

Substituting the equation (26) into equation (25) yields

$$\ddot{\eta}_s + \sum_{m=0}^{M} (\omega_s^2 \delta_{sm} + T_{sm}/N_s)\eta_m = \frac{1}{\rho_b A_b N_s} \int_b^a f(r, t) R_s(r)\, \mathrm{d}r, \qquad s = 0, 1, 2, \ldots, M, \tag{27}$$

where ω_s is the sth natural frequency of the beam and

$$T_{sm} = \frac{1}{\rho_b A_b} \int_b^a k(r) R_m(r) R_s(r)\, \mathrm{d}r, \qquad N_s = \int_b^a R_s^2(r)\, \mathrm{d}r. \tag{28, 29}$$

If k is a constant, the modal equations are uncoupled, becoming

$$\ddot{\eta}_s + \left(\omega_s^2 + \frac{k}{\rho_b A_b}\right)\eta_s = \frac{1}{\rho_b A_b N_s}\int_b^a f(r, t)R_s(r)\,\mathrm{d}r, \qquad s = 0, 1, 2, \ldots, M. \tag{30}$$

4. FREQUENCIES OF THE BEAM-SUPPORTED PLATE

A beam-supported rotating plate can be decomposed into three subsystems as shown in Figure 2. The receptance method is applied here to join the rotating plate and the beam supports. To apply the receptance method for structural combination, one requires the structures to have the same shape functions on the connecting line. This is the reason for the beam functions being used for both beam and plate. It is realized that the radial dependence of the plate shape functions is slightly different from that of the beam. The errors are, however, corrected through the boundary residuals and the approach yields accurate results.

Upon assuming a harmonic line load of the distribution, $R_0(r)$ to be applied on the beam, as shown in Figure 3, one has

$$f(r, t) = FR_0(r)\,\mathrm{e}^{\mathrm{i}\omega t}, \tag{31}$$

and the beam's response is obtained as

$$u(r, t) = \frac{FR_0(r)}{\rho_b A_b(\omega_0^2 - \omega^2) + k}\,\mathrm{e}^{\mathrm{i}\omega t}, \tag{32}$$

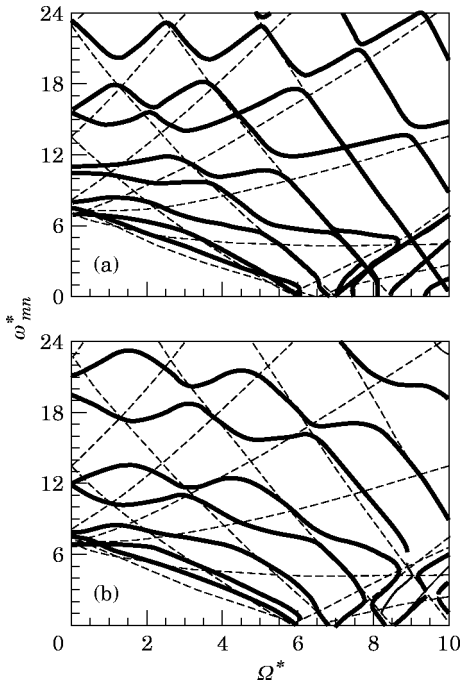

Figure 7. Variations of natural frequencies with rotation speeds for $L = 2$, asymmetric placement. (a), (b) as Figure 4.

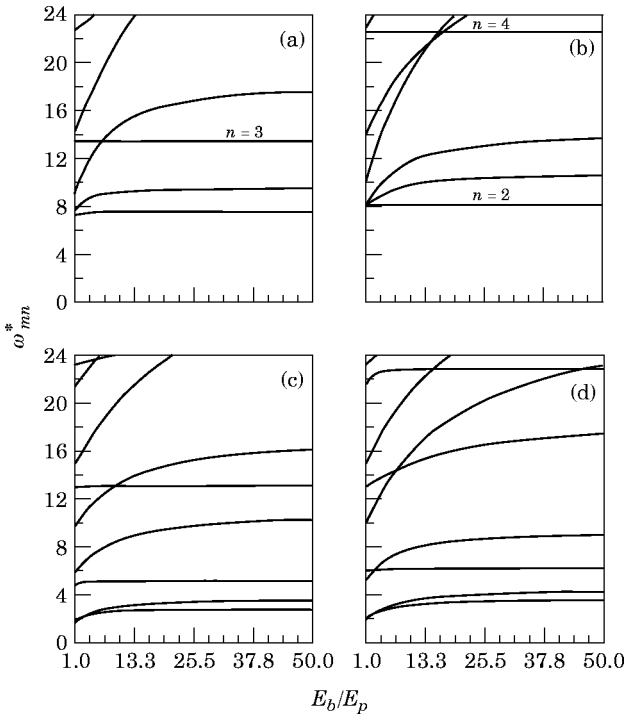

Figure 8. Variations of frequencies with stiffness ratios. L, Ω^* values: (a) 3, 0; (b) 4, 0; (c) 3, 5; (d) 4, 5.

where ω_0 denotes the beam's $m = 0$ natural frequency. Note that $f(r, t)$ is a line load and can be directly applied to the beam equation to give its response. To apply it to the plate, a corresponding pressure type load is first derived, i.e.,

$$q(r, \phi, t) = \frac{FR_0(r)}{r}\,\delta(\phi - \phi_i)\,\mathrm{e}^{\mathrm{i}\omega t}, \tag{33}$$

where $\delta(\phi - \phi_i)$ denotes the ith support location. Likewise, the plate response due to the ith line load is obtained as

$$u(r, \phi, t) = \frac{1}{\rho_p h_p \pi}\sum_{n=0}^{N}\frac{FN_0R_0(r)\,\mathrm{e}^{\mathrm{i}\omega t}}{\kappa\Gamma_{0n}(\omega^2 - \omega_{n1}^2)(\omega_{n2}^2 - \omega^2)}\{(\omega_{n1}\omega_{n2} + \omega^2)\cos[n(\phi - \phi_i)]$$

$$-\mathrm{i}\omega(\omega_{n2} + \omega_{n1})\sin[n(\phi - \phi_i)]\}, \tag{34}$$

where $\kappa = 2$ for $n = 0$ and $\kappa = 1$ for $n \neq 0$. $\omega_{n1}, \omega_{n2} = n\Omega \mp \Psi_n$ denote the $(0, n)$ natural frequencies of the rotating plate.

Subsequently, the receptances of the beam, denoted β, and of the spinning plate, denoted α, are obtained as

$$\beta_{ii} = 1/\{\rho_b A_b(\omega_0^2 - \omega^2) + k\}, \qquad \beta_{ij} = 0, \tag{35}$$

and

$$\alpha_{ii} = \frac{N_0}{\rho_p h_p \pi}\sum_{n=0}^{N}\frac{(\omega_{n1}\omega_{n2} + \omega^2)}{\kappa\Gamma_{0n}(\omega^2 - \omega_{n1}^2)(\omega_{n2}^2 - \omega^2)}, \qquad \alpha_{ji} = R_{ji}(\omega) + \mathrm{i}I_{ji}(\omega), \tag{36, 37}$$

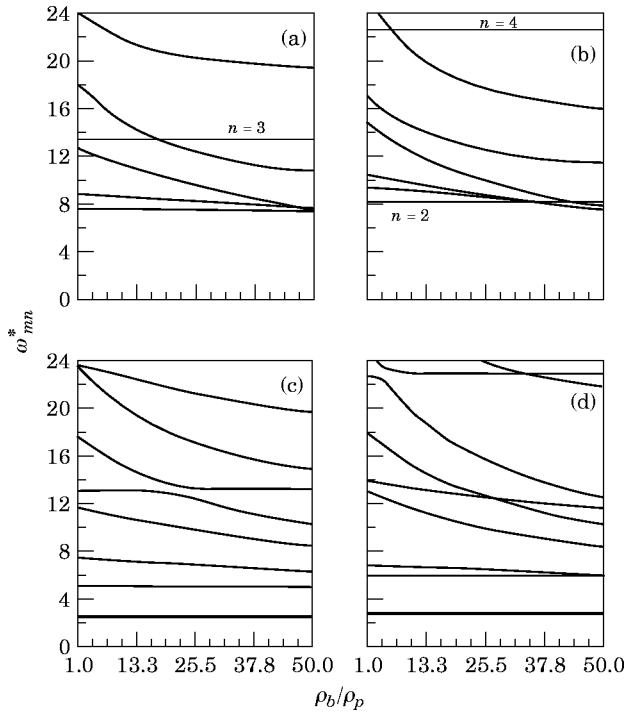

Figure 9. Variations of frequencies with inertia ratios. (a)–(d) as Figure 8.

where

$$R_{ji} = \frac{N_0}{\rho_p h_p \pi} \sum_{n=0}^{N} \frac{(\omega_{n1}\omega_{n2} + \omega^2)\cos[n(\phi_j - \phi_i)]}{\kappa \Gamma_{0n}(\omega^2 - \omega_{n1}^2)(\omega_{n2}^2 - \omega^2)}, \tag{38}$$

$$I_{ji} = \frac{N_0}{\rho_p h_p \pi} \sum_{n=0}^{N} \frac{\omega(\omega_{n2} + \omega_{n1})\sin[n(\phi_j - \phi_i)]}{\kappa \Gamma_{0n}(\omega^2 - \omega_{n1}^2)(\omega_{n2}^2 - \omega^2)}. \tag{39}$$

The beam's cross-receptances are zero, since the beams are assumed to be connected to a rigid shaft and therefore no interaction occurs. The cross-receptances of the plate are in complex conjugate pairs. This property was discovered by Huang and Hsu through the

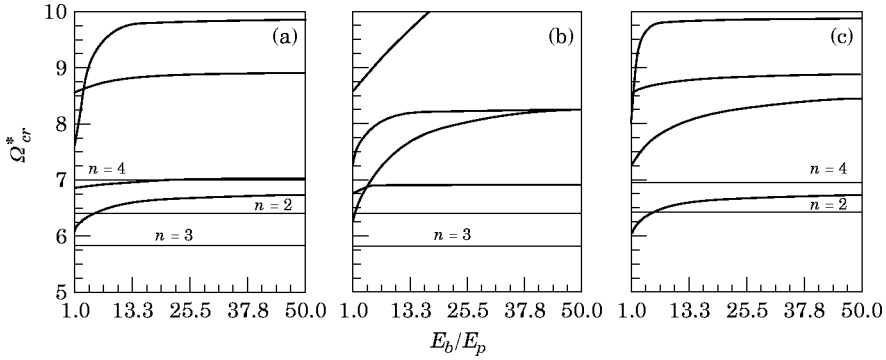

Figure 10. Variance of critical speeds with supports stiffness. L values: (a) 2; (b) 3; (c) 4.

investigation of a rotating plate [14] and a rotating shell [19]. Now, employing the compatibility and equilibrium conditions at the connections [20], the frequency equation of the rotating plate with L symmetrical beam-supports is obtained as

$$\begin{vmatrix} [\Pi(\omega)]_{L\times L} & [\Pi^c(\omega)]_{L\times L} \\ [\Pi^c(\omega)]_{L\times L} & [\Pi(\omega)]_{L\times L} \end{vmatrix} = 0, \tag{40}$$

where

$$\Pi_{ii} = \alpha_{ii} + \beta_{ii}, \qquad \Pi_{ij} = \alpha_{ij}, \qquad \Pi^c_{ij} = \alpha_{ij}. \tag{41}$$

The frequencies that satisfy equation (40) are the natural frequencies of the beam-supported rotating plate.

5. EXAMPLES

The material and geometric properties of the plate and beam are listed in Table 2. The individual frequencies of the beam and the plate are given in Table 3. Note that the beam's first frequency was calculated with respect to the plate's neutral surface. The frequencies show that the beam's first frequency falls above the plate's $n = 2$ frequency. From the theory of receptance it is expected that, after combination, the plate's lower few frequencies will be raised by the beam-supports. As the plate rotates its backward frequencies decrease with rotation and the beam's stiffening effects become more significant.

Numerical solutions of equation (40) for $L = 2, 3, 4$ are illustrated in Figures 4–6, to show the vibration characteristics. These figures show the variations of the beam-supported plate's natural frequencies (solid curves) with the rotation speed for (a) a relatively low k (2000 $\mathrm{N/m^2}$) and (b) rigid supports ($k = \infty$). Since the beams were designed to stiffen the plate, the authors here let the beam be five times more rigid than the plate to emphasize the effects: i.e., $E_b = 5E_p$ and $\rho_b = \rho_p$. The effects of mass ratios and stiffness ratios will be discussed in a later section. The natural frequencies (dashed curves) of the rotating plate are superimposed on to the plots for comparison.

From Figure 4, it is first noticed that at no rotation the supported plate has almost double the number of natural frequencies. In fact, except for the $n = 0$ mode, there are two natural frequencies associated with each n number, in which one is the same as that of the non-supported plate and the other, of higher value, is generated from the supports. This phenomenon is due to the supports destroying the degeneracy of the plate frequencies. In a plate, there are two modes, $\sin(n\theta)$ and $\cos(n\theta)$, associated with each $n \neq 0$ natural frequency. When supports are imposed on the plate one of the modes, say $\sin(n\theta)$, orients itself such that the supports coincide with the nodal diameters. Therefore, the original frequency remains. Simultaneously, the other mode, say $\cos(n\theta)$, has the supports on its anti-nodes and hence a higher frequency.

As to the frequency variations with rotation speed, the frequency curves show veering and mode exchange phenomena. These curves separate farther apart as the supports stiffness increases. These phenomena are seen in the point-supports cases too [14].

Some features shown in the figures are worthy of discussion. First, the intersections of frequency curves with the abscissa correspond to the critical speeds of the plate. As the

plate is running at one of the critical speeds, the corresponding mode becomes a standing wave and the plate undergoes a divergent type instability. The unsupported rotating plate in the examples has its critical speeds at $\Omega_p^* = 5{\cdot}85$ ($n = 3$), $6{\cdot}4$ ($n = 2$) and $7{\cdot}0$ ($n = 4$), . . . , etc. In Figures 4 and 5 it is shown that in the $L = 2, 3$ cases the first critical speed remains at $5{\cdot}85$, since in both cases the $n = 3$ plate mode is retained. Thus, the supports do not improve the critical speed. In the $L = 4$ case, the first critical speed shifts to the $n = 2$ mode, since the four rigid supports require four nodal diameters and therefore the original $n = 3$ mode cannot exist. It is hence realized that the number of supports should be appropriately chosen if improving the critical speed is the main issue. The guideline for choosing an appropriate number of supports is that $L \neq n_c$ and $L \neq 2n_c$, where n_c is the first critical mode. For example, the current plate shows the first critical mode at $n = 3$, and therefore the number of supports cannot be three or six. Moreover, if the second critical mode ($n = 2$) needs to be shifted, L cannot be 2 or 4. Another alternative for improving critical speeds is to place the supports asymmetrically. For instance, Figure 7 shows the $L = 2$ case with two supports separated by 150 degrees. The first critical speed is slightly lifted to around $6{\cdot}0$.

Moreover, it is interesting that the beam-supported rotating plate has more critical speeds than the free rotating plate. This means that the supports induce more instabilities. Similar phenomena were observed in the investigation of a rotating plate with point supports [14, 21].

The second interesting feature is that the frequency curves pass through some but not all of the crossings of the dashed curves: i.e., the plate's natural frequencies remain those of the beam-supported plate. The rules of justification being developed by Huang and Hsu [9] for a circular cylindrical shell with point supports apply to the present system as well. Let n_1 and n_2 be the n numbers of the two curves. Consider case (i), in which n_1 and n_2 are both forward modes or backward modes. Then if $|n_1 - n_2|$ is an integer multiple of L, the cross-frequency remains as a natural frequency of the supported plate. For case (ii), in which n_1 and n_2 are one forward and one backward mode, the cross-frequency remains if $(n_1 + n_2)$ is an integer multiple of L.

The third feature observed is that some of the frequency curves start to turn over as the plate reaches certain rotating speeds ($\Omega^* > 7{\cdot}0$). At the turning points the sensitivity (ω^* versus Ω^*) approaches infinity. This is why the curves show scattering in these regions. When the rotation speed exceeds that point the eigenvalues become complex with positive real parts and the plate experiences flutter instability. Those roots are not shown in the figures since it has been assumed from the beginning in the receptance method that the system is undergoing harmonic motion (imaginary roots).

In Figure 8 are shown the stiffness ratio effects for $\Omega^* = 0$ and 5, with $\rho_b = \rho_p$. It is first seen for $\Omega^* = 0$ that the $n = 3$ mode in $L = 3$ and $n = 2, 4$ modes in $L = 4$ remain unchanged with stiffness ratios since the supports are located on the nodal diameters. However, this phenomenon disappears when the plate rotates because the modes become traveling ones and the nodal lines no longer fixed in space (except at critical speeds). The figures show that there are more curves in $\Omega^* = 5$ due to frequency bifurcations. The curves also show that the stiffness ratios affect the higher n modes more than the lower modes.

The mass ratio effects with $E_b = 5E_p$ are shown in Figure 9. As in Figure 8, the mass affects higher modes more than the lower modes. The variations of critical speeds with the stiffness ratios are illustrated in Figure 10. It is seen that in the $L = 2$ figure, the critical speeds associated with $n = 3$ and 2 are not affected by the supports. The first critical speed appears for $n = 3$ in the $L = 2$ or 3 cases and appears for $n = 2$ in the $L = 4$ case.

6. CONCLUSIONS

The natural frequencies of a rotating plate with two-side beam-supports have been investigated. The approach employs a mixed weighted residual method and the receptance method. Numerical examples for $L = 2, 3$ and 4 are illustrated. The results show that the beam supports raise the plate's first three natural frequencies provided that the beam is of the same material and thickness as the plate. As the rigidity of the beams is increased via increasing E or the thickness, more of the plate frequencies are increased. The attachment of the beams destroys the originally degenerate plate modes and results in more distinct natural frequencies. The improvement of the critical speed depends on the number of beams being selected. If none of the supports coincide with the nodal diameters of the first critical mode, the beam-supports can improve the first critical speed. The supports, however, also induce more critical speeds after the first critical speed. The effects of stiffness and inertia ratios were also studied and the results show that the higher modes are affected more by the supports.

REFERENCES

1. H. Lamb and R. V. Southwell 1921 *Proceedings of the Royal Society*, *London* **99**, 272–280. The vibrations of a spinning disk.
2. C. D. Mote Jr. 1965 *Transactions of the American Society of Mechanical Engineers*, *Journal of Engineering for Industry* **87**, 258–264. Free vibrations of initially stressed circular disks.
3. G. K. Ramaiah 1981 **74**(2), 303–310. Natural frequencies in spinning annular plates.
4. G. G. Adams 1987 *International Journal of Mechanical Science* **29**, 525–531. Critical speed for a flexible spinning disk.
5. I. Y. Shen and C. D. Mote Jr. 1991 *Journal of Sound and Vibration* **148**, 307–318. On the mechanisms of instability of a circular plate under a rotating spring–mass–dashpot system.
6. J. S. Chen and D. B. Bogy 1992 *Transactions of the American Society of Mechanical Engineers*, *Journal of Applied Mechanics* **59**, S230–S235. Effects of load parameters on the natural frequencies and stability of a flexible spinning disk with a stationary load system.
7. J. S. Chen and D. B. Bogy 1992 *Transactions of the American Society of Mechanical Engineers*, *Journal of Applied Mechanics* **59**, 390–397. Mathematical structure of modal interactions in a spinning disk–stationary load system.
8. A. W. Leissa and C. L. Kirk 1967 *Journal of Sound and Vibration* **5**, 278–284. Vibrations characteristics of a circular plate with a concentric reinforcing ring.
9. S. K. Sinha 1988 *Transactions of the American Society of Mechanical Engineers*, *Journal of Vibration and Acoustics*, *Stress and Reliability in Design* **110**, 507–514. On free vibrations of a thin spinning disk stiffened with an outer reinforcing ring.
10. H. C. Loh and J. F. Carney III 1977 *Journal of Applied Mechanics* 499–501. Vibration and stability of spinning annular plates reinforced with edge beams.
11. S. Azimi 1988 *Journal of Sound and Vibration* **120**, 19–35. Free vibration of circular plates with elastic edge supports using the receptance method.
12. S. Azimi 1988 *Journal of Sound and Vibration* **120**, 37–52. Free vibration of circular plates with elastic or rigid interior supports.
13. S. Azimi 1989 *Journal of Sound and Vibration* **135**, 177–195. Axisymmetric vibration of point-supported circular plates.
14. S. C. Huang and B. S. Hsu 1992 *Transactions of the American Society of Mechanical Engineers*, *Journal of Vibration and Acoustics* **114**, 468–476. Receptance theory applied to modal analysis of a spinning disk with interior multi-point supports.
15. S. C. Huang and B. S. Hsu 1993 *Journal of Sound and Vibration* **164**, 535–547. Vibration of spinning annular plate with multi-circular line guides.
16. S. G. Hutton, S. Chonan and B. F. Lehmann 1987 *Journal of Sound and Vibration* **112**, 527–539. Dynamic response of a guided circular saw.

17. S. C. Huang and W. J. Chiou 1994 *Transactions of the American Society of Mechanical Engineers*, *Journal of Vibration and Acoustics* **115**, 535–543. Modeling and vibration analysis of spinning-disk and moving-head assembly.
18. S. M. Vogel and D. W. Skinner 1965 *Journal of Applied Mechanics* **32**, 926–931. Natural frequencies of transversely vibrating uniform annular plates.
19. S. C. Huang and B. S. Hsu 1993 *Transactions of the American Society of Mechanical Engineers*, *Journal of Vibration and Acoustics* **115**, 535–543. Modal analysis of a spinning cylindrical shell with interior point or circular line supports.
20. R. E. D. Bishop and D. C. Johnson 1960 *The Mechanics of Vibration*. Cambridge: Cambridge University Press.
21. C. D. Mote Jr. 1977 *Journal of Acoustical Society of America* **61**(2), 439–447. Moving-load stability of a circular plate on a floating central collar.